

Journal of Materials Chemistry C

Accepted Manuscript



This is an *Accepted Manuscript*, which has been through the Royal Society of Chemistry peer review process and has been accepted for publication.

Accepted Manuscripts are published online shortly after acceptance, before technical editing, formatting and proof reading. Using this free service, authors can make their results available to the community, in citable form, before we publish the edited article. We will replace this *Accepted Manuscript* with the edited and formatted *Advance Article* as soon as it is available.

You can find more information about *Accepted Manuscripts* in the [Information for Authors](#).

Please note that technical editing may introduce minor changes to the text and/or graphics, which may alter content. The journal's standard [Terms & Conditions](#) and the [Ethical guidelines](#) still apply. In no event shall the Royal Society of Chemistry be held responsible for any errors or omissions in this *Accepted Manuscript* or any consequences arising from the use of any information it contains.

A novel regrowth mechanism and enhanced optical properties of $\text{Mg}_{0.25}\text{Zn}_{0.75}\text{O}$ nanorod subjected to vapor-confined face-to-face annealing

Cite this: DOI: 10.1039/x0xx00000x

Received 00th January 2012,
Accepted 00th January 2012

DOI: 10.1039/x0xx00000x

www.rsc.org/

Giwoong Nam,^a Byunggu Kim,^a Youngbin Park,^a Seonhee Park,^a Jiyun Moon,^a Do Yeob Kim,^b Sung-O Kim^b and Jae-Young Leem^{*a}

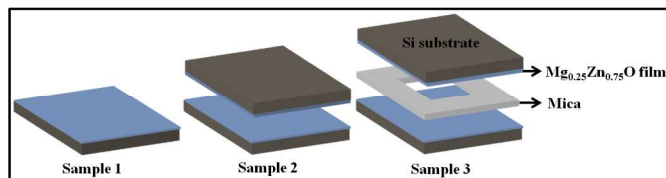
Although the sol-gel spin-coating method is usually a technique for depositing thin films, here, we report on the sol-gel fabrication of one-dimensional $\text{Mg}_{0.25}\text{Zn}_{0.75}\text{O}$ nanorods through the use of vapor-confined face-to-face annealing (VC-FTFA), in which mica is inserted between two films before annealing using the FTFA method. $\text{Mg}_{0.25}\text{Zn}_{0.75}\text{O}$ nanorods are regrown when magnesium chloride hexahydrate is used as the solvent, because ZnCl_2 and MgCl_2 vapors are generated under these conditions. The near-band-edge emission intensity of the $\text{Mg}_{0.25}\text{Zn}_{0.75}\text{O}$ nanorods is enhanced by the VC-FTFA by a factor of 37 compared to that of the films annealed in open air at 700 °C. Our method may provide a route for the facile fabrication of $\text{Mg}_{0.25}\text{Zn}_{0.75}\text{O}$ nanorods.

Introduction

One-dimensional (1D) nanostructures, including nanorods, nanowires, and nanotubes, have aroused considerable research interest in many areas of nanoscience and nanotechnology. There are two reasons for this interest: first, 1D nanostructures have unusual and unique physical properties, such as quantum-mechanical confinement effects (QCE)^{1–3} and a high surface-to-volume ratio making them relevant for the development of new devices and sensors.^{4–6} In particular, it is believed that QCE plays a crucial role in improving the optical properties of materials.⁷ In particular, the wide-band-gap wurtzite semiconductors have attracted much attention because of their potential applications for optoelectronic devices emitting light in the blue and ultraviolet (UV) regions. ZnO have been proposed as a wide-band-gap (3.37 eV) semiconductor for short-wavelength optoelectronic applications such as light-emitting diodes (LEDs).^{8,9} One of the interesting features of ZnO is the possibility of tuning its band gap by substituting (alloying) bivalent metals such as Cd and Mg in place of Zn. While Cd is known to reduce the band gap,¹⁰ Mg substitution widens it.¹¹ To obtain high-performance LED devices, the key technique is to fabricate a heterojunction to confine both electrons and photons. To form this heterojunction, one possible material is MgO, which has a band-gap energy of 7.8 eV and a cubic crystal structure. Alloying of ZnO with MgO should not cause significant changes in the lattice constants, because the ionic radius of Mg^{2+} (0.57 Å) is similar to that of

Zn^{2+} (0.60 Å). Therefore, the $\text{Mg}_{0.25}\text{Zn}_{0.75}\text{O}$ alloy system is considered to be a suitable potential barrier material.

There are many techniques for preparing $\text{Mg}_x\text{Zn}_{1-x}\text{O}$ nanorods, such as metal-organic chemical vapor deposition, chemical vapor deposition, molecular beam epitaxy, and vapor phase transport.^{12–15} Another option is the sol-gel method, which is conventionally not a 1D nanostructure growth technique but rather a thin film deposition technique. If it could be adapted to the growth of nanorods, this method would provide advantages such as reproducibility, low cost, and mass production capability for uniform large-area coatings. However, in most studies, $\text{Mg}_x\text{Zn}_{1-x}\text{O}$ deposited through solution routes method exhibits poor optical properties.^{16–19} One supplemental approach could be the face-to-face annealing (FTFA) technique, which is commonly employed for GaAs semiconductor fabrication to prevent out-diffusion of arsenic.²⁰ The GaAs wafer to be annealed is placed between a bottom Si wafer and a top GaAs wafer with the polished surfaces facing each other, which is why this approach is called the FTFA. Wang *et al.*²¹ found that photoluminescence (PL) properties of ZnO thin films were enhanced by FTFA. In this paper, we used sol-gel spin-coating and a new annealing method called vapor-confined FTFA (VC-FTFA) to fabricate $\text{Mg}_{0.25}\text{Zn}_{0.75}\text{O}$ nanorods using magnesium chloride hexahydrate for regrowth. This method has several advantages over the conventional FTFA method. For example, it produces a sharp increment in the near-band-edge (NBE) emission intensity in the PL spectra. Here, we describe



Scheme 1 Annealing configuration for annealing in the open air (sample 1), conventional FTFA (sample 2), and FTFA with an additional mica film inserted between the two layers (sample 3).

the mechanism for the generation of vapors during annealing and the influence of confined vapor on the optical properties of $\text{Mg}_{0.25}\text{Zn}_{0.75}\text{O}$ nanorods.

Experimental

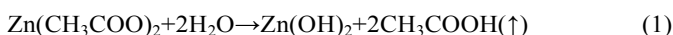
$\text{Mg}_{0.25}\text{Zn}_{0.75}\text{O}$ films were deposited onto Si substrate by sol-gel spin-coating method. The precursor solutions for the $\text{Mg}_{0.25}\text{Zn}_{0.75}\text{O}$ films were prepared from zinc acetate dihydrate ($\text{Zn}(\text{CH}_3\text{COO})_2 \cdot 2\text{H}_2\text{O}$, ACS Reagent, >98%, Sigma-Aldrich) and magnesium chloride hexahydrate ($\text{MgCl}_2 \cdot 6\text{H}_2\text{O}$, >98%, JUNSEI) dissolved in 2-methoxyethanol (99.8%, Sigma-Aldrich) as solvent. The concentration of the metal precursors was 0.5 M. Monoethanolamine ($\text{C}_2\text{H}_7\text{NO}$, MEA, ACS Reagent, >99.0%, Sigma-Aldrich) was used as a stabilizing agent to improve the solubility of the precursor salt. The molar ratio of MEA to metal salts was 1.0, and the ratio of Mg to Zn was fixed at 25 at.%. The stabilized sol solution was stirred at 60 °C for 2 h until it became clear and homogeneous. It was subsequently cooled to RT and aged for 24 h before it was used as the coating solution to deposit the films.

The Si substrates were ultrasonically cleaned in acetone and ethanol for 10 min, rinsed with deionized water, and blow-dried with nitrogen. The precursor solution was spin-coated onto a Si substrate at 2000 rpm for 20 s, and then the films were dried at 200 °C for 10 min in an oven. These spin-coating and drying procedures were repeated five times. The basic strategy for annealing of $\text{Mg}_{0.25}\text{Zn}_{0.75}\text{O}$ films is shown in Scheme 1. Three samples were prepared for a comparative study at 700 °C: Three samples were prepared at 500 °C for a comparative study. Sample 1 was annealed in open air. Sample 2 was annealed by the conventional FTFA method, in which two films are placed together FTF during annealing. For sample 3, mica was inserted between the two films annealed by the FTFA method.

The PL properties of $\text{Mg}_{0.25}\text{Zn}_{0.75}\text{O}$ were measured using the photocount method with a He-Cd excitation laser (325 nm) with a power of 20 mW and a 0.75-m single-grating monochromator with a photomultiplier tube (HAMAMATSU, R928). The surface morphology was analyzed using a field-emission scanning electron microscope (FE-SEM, HITACHI, S-4800). The thermal analysis of the $\text{Mg}_{0.25}\text{Zn}_{0.75}\text{O}$ precursors was performed using a thermogravimetry-differential thermal analyzer (TG-DTA, TA Instruments, SDT Q600) system at a heating rate of 10 °C/min in air. The crystal phase of the $\text{Mg}_x\text{Zn}_{1-x}\text{O}$ films was investigated using an X-ray diffractometer (PANalytical X'Pert Pro, the Netherlands) with a Cu-K α radiation source ($\lambda = 0.154056 \text{ \AA}$) and an accelerating voltage of 40 kV.

Results and discussion

The thermal-decomposition behaviors of the ZnO and $\text{Mg}_{0.25}\text{Zn}_{0.75}\text{O}$ precursors were determined using a TG-DTA, in which the materials were heated from room temperature to 700 °C at a constant rate of 10 °C/min in air. Fig. 1 shows the TG-DTA curves of the ZnO and $\text{Mg}_{0.25}\text{Zn}_{0.75}\text{O}$ precursors, which both exhibit an initial weight loss at 100 °C resulting from the evaporation of the solvent and water. In addition, the ZnO precursors exhibited weight losses in the temperature regions of 100 – 220 and 220 – 250 °C, and the $\text{Mg}_{0.25}\text{Zn}_{0.75}\text{O}$ precursors exhibited weight losses at 100 – 250, 250 – 350, and 350 – 610 °C. These weight losses were all attributed to the decomposition of organic compounds. Specifically, in the temperature region of 350 – 610 °C, the $\text{Mg}_{0.25}\text{Zn}_{0.75}\text{O}$ precursor slowly evaporated, which generated ZnCl_2 and MgCl_2 vapors, as described by the following reactions:



The ZnO and $\text{Mg}_{0.25}\text{Zn}_{0.75}\text{O}$ precursors exhibited endothermic and exothermic peaks between 25 and 300 °C and between 25 and 550 °C, respectively, in the heat flow analysis, which were attributed to the evaporation of water and organics from these precursors. The last exothermic peaks in the TG-DTA curves of the ZnO and $\text{Mg}_{0.25}\text{Zn}_{0.75}\text{O}$ precursors, at 360 and 600 °C, respectively, resulted from the crystallization of ZnO and $\text{Mg}_{0.25}\text{Zn}_{0.75}\text{O}$.

Sample 1 consisted of numerous round-shaped $\text{Mg}_{0.25}\text{Zn}_{0.75}\text{O}$ nanoparticles of approximately 50 nm in diameter, as shown in the SEM image in Fig. 2a. Large $\text{Mg}_{0.25}\text{Zn}_{0.75}\text{O}$ particles (~200 nm)

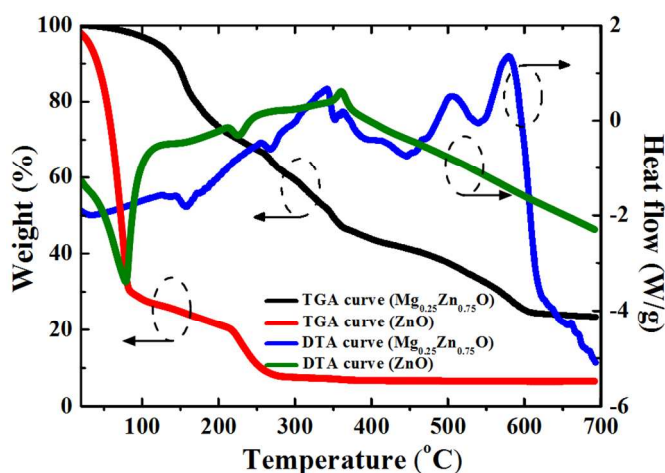


Fig. 1 TGA and DTA curves, shown as the percentage of weight loss and the heat flow, respectively, for the ZnO and $\text{Mg}_{0.25}\text{Zn}_{0.75}\text{O}$ precursors.

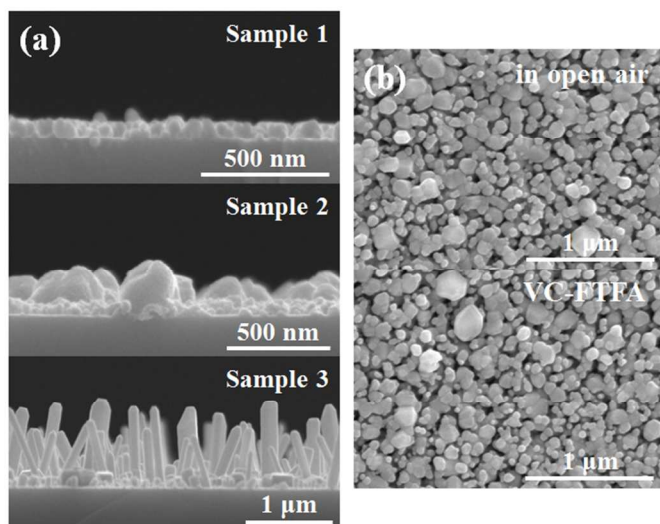


Fig. 2 (a) SEM images of the three samples and (b) $\text{Mg}_{0.25}\text{Zn}_{0.75}\text{O}$ films prepared using a magnesium acetate tetrahydrate precursor as the dopant annealed in open air or using the VC-FTFA method at 700°C .

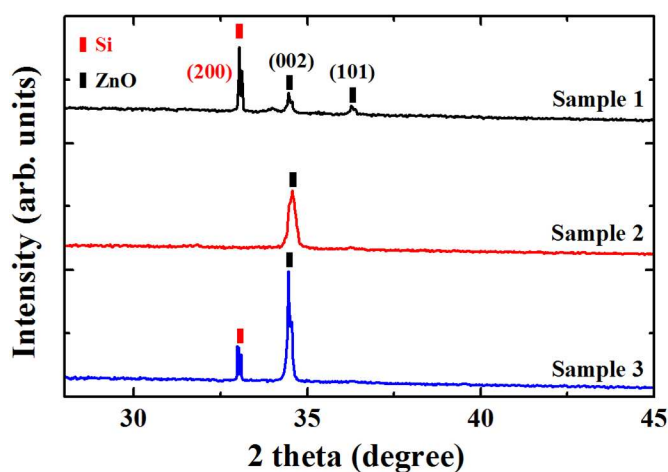
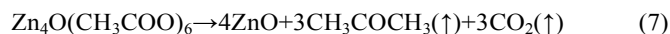


Fig. 3 XRD analysis of the three samples.

were formed on the $\text{Mg}_{0.25}\text{Zn}_{0.75}\text{O}$ nanoparticles in sample 2, and $\text{Mg}_{0.25}\text{Zn}_{0.75}\text{O}$ nanorods were grown using the VC-FTFA method in sample 3. These large particles and nanorods were assembled from the round-shaped $\text{Mg}_{0.25}\text{Zn}_{0.75}\text{O}$ nanoparticles because of the role of the nucleation agents in the seed layer. ZnCl_2 and MgCl_2 vapors were generated in the temperature region of $350 - 610^\circ\text{C}$, and round-shaped nanoparticles were regrown from the ZnCl_2 and MgCl_2 vapors. The regrowth of the large $\text{Mg}_{0.25}\text{Zn}_{0.75}\text{O}$ particles and nanorods can be attributed to the vapor-solid mechanism, in which the large particles and nanorods grow via the oxidation of the produced Zn and Mg vapors, followed by condensation. The ZnCl_2 and MgCl_2 vapors were generated and decomposed in the temperature range of $350 - 610^\circ\text{C}$, and $\text{Mg}_{0.25}\text{Zn}_{0.75}\text{O}$ nanorods were formed on the round-shaped nanoparticles from organic compounds that contained oxygen or from oxygen present in the air. However, the surface morphology did not change when $\text{Mg}_{0.25}\text{Zn}_{0.75}\text{O}$ films were prepared using the magnesium acetate

tetrahydrate as a dopant (Fig. 2b). As the temperature increased, the zinc acetate dihydrate gradually decomposed to form ZnO through the following chemical reactions:²²



The chemical reactions of magnesium acetate tetrahydrate are similar to those of zinc acetate dihydrate. Therefore, according to chemical reactions (4-7), an acetate-based solvent cannot generate vapors that facilitate regrowth and the $\text{Mg}_{0.25}\text{Zn}_{0.75}\text{O}$ nanorods formed by regrowth when a chloride-based solvent was used because ZnCl_2 and MgCl_2 vapors were generated.

Fig. 3 shows the X-ray diffraction patterns of the three samples. Two ZnO diffraction peaks were observed at 34° and 36° , which correspond to the (002) and (101) planes, respectively. No traces of Mg metal or oxide were detected, indicating that the wurtzite structure was not modified by the incorporation of Mg into the ZnO matrix. Sample 2 and 3 exhibited a strong (002) peak, indicating that the c-axis orientation of the ZnO grains was perpendicular to the substrate. It was also observed that the intensity of the (002) peak in sample 3 was larger than that in sample 2.

Fig. 4a presents optical images of the three samples illustrated in Scheme 1. Sample 1 was transparent, whereas samples 2 and 3 were covered with white-colored products on the surfaces of the Si substrates. We evaluated the degree of uniformity of the NBE emission intensities in the PL spectra at the circles marked in the red in Fig. 4a on the three samples (Fig. 4b) using a continuous-wave helium-cadmium (He-Cd) laser as the optical excitation source. The NBE emission intensities were randomly distributed over the entire surface of sample 1, whereas those of sample 2 were stronger on the edges of the surface than in the center, because the generated ZnCl_2 and MgCl_2 vapors were not sufficiently confined. These vapors

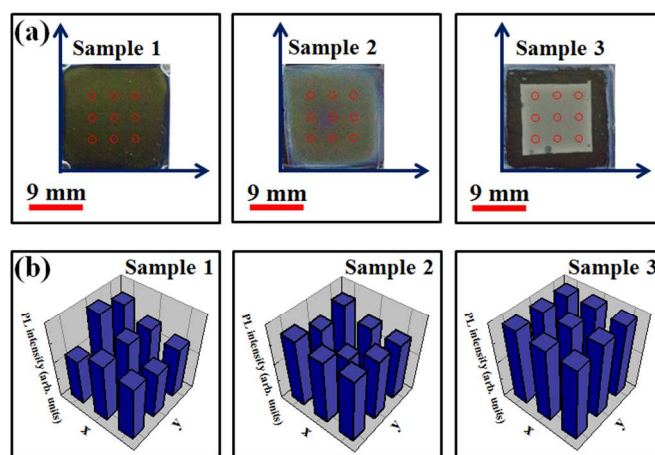


Fig. 4 (a) Optical images of the three samples, which are $18 \times 18 \text{ mm}^2$ in size. (b) Degree of uniformity of the NBE emission intensities. The PL spectra were measured in the regions of the red circle in Fig. 4a.

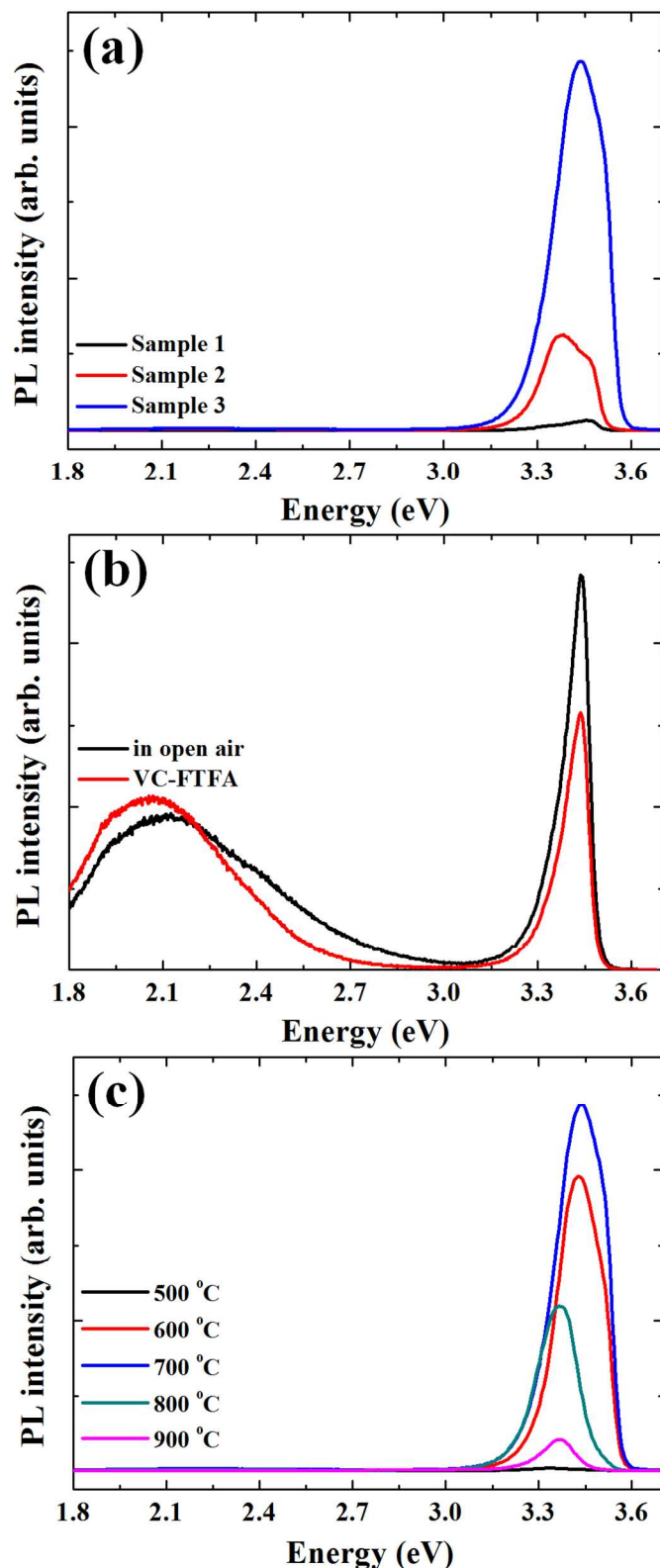


Fig. 5 PL spectra of (a) the three samples, (b) $\text{Mg}_{0.25}\text{Zn}_{0.75}\text{O}$ films fabricated using a magnesium acetate tetrahydrate precursor as the dopant and were annealed in open air (black line) or using the VC-FTFA (red line) method at 700 °C, and (c) $\text{Mg}_{0.25}\text{Zn}_{0.75}\text{O}$ nanorods annealed at various temperatures using the VC-FTFA method.

remained briefly at the center of the surface, and round-shaped nanoparticles were slightly regrown. For sample 3, however, the NBE emission intensities appeared to be evenly distributed over the entire surface, because the vapors were confined by the mica. We attribute the active regrowth to the confinement of these vapors.

Fig. 5a presents the PL spectra of the three samples. The NBE emission intensity was clearly enhanced by annealing using the VC-FTFA method, by a factor of 37 compared to that of the films annealed in open air. The enhanced NBE emission intensity might be attributed to the decrease of the nonradiative recombination defect by Mg incorporation and the enhancement of crystallinity through regrowth reaction. Therefore, the regrowth resulting from the VC-FTFA method is effective in increasing not only the NBE emission intensity but also the emission uniformity. For the $\text{Mg}_{0.25}\text{Zn}_{0.75}\text{O}$ films annealed in open air that were deposited using a magnesium acetate tetrahydrate precursor as the dopant, which cannot generate vapor that facilitate regrowth, the NBE emission intensity was higher than that of the $\text{Mg}_{0.25}\text{Zn}_{0.75}\text{O}$ films annealed using VC-FTFA method (Fig. 5b). The spectra of the two samples contain a yellow-orange emission band at approximately 2.2 eV that originates from interstitial oxygen ions (O_i^-).²³

Fig. 5c presents the PL spectra of $\text{Mg}_{0.25}\text{Zn}_{0.75}\text{O}$ films that were annealed using the VC-FTFA method with various annealing temperatures. As the annealing temperature was increased to 700 °C, the NBE emission intensity also increased. The NBE emission intensity of the film annealed at 500 °C was the lowest, because ZnCl_2 and MgCl_2 vapors were generated and decomposed only minimally under these conditions. At an annealing temperature of 700 °C, ZnCl_2 and MgCl_2 vapors were fully generated and decomposed, and these vapors remained between the $\text{Mg}_{0.25}\text{Zn}_{0.75}\text{O}$ films and caused active regrowth. The NBE emission intensity, however, decreased when the annealing temperature was increased to 900 °C because the ZnCl_2 and MgCl_2 vapors activated by the thermal energy were not well confined and escaped from the region between the $\text{Mg}_{0.25}\text{Zn}_{0.75}\text{O}$ films.

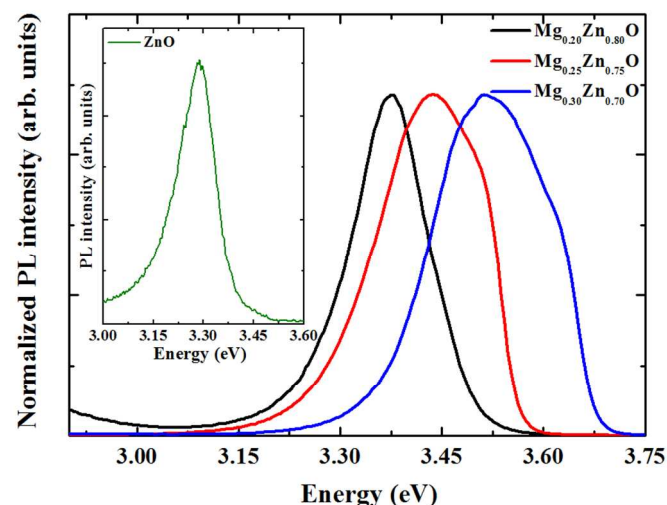


Fig. 6 Normalized PL spectra of $\text{Mg}_x\text{Zn}_{1-x}\text{O}$ nanorods with various Mg contents ($x = 0.20, 0.25, \text{ and } 0.30$) using VC-FTFA at 700 °C. The inset shows the PL spectrum of ZnO films annealed in open air at 700 °C.

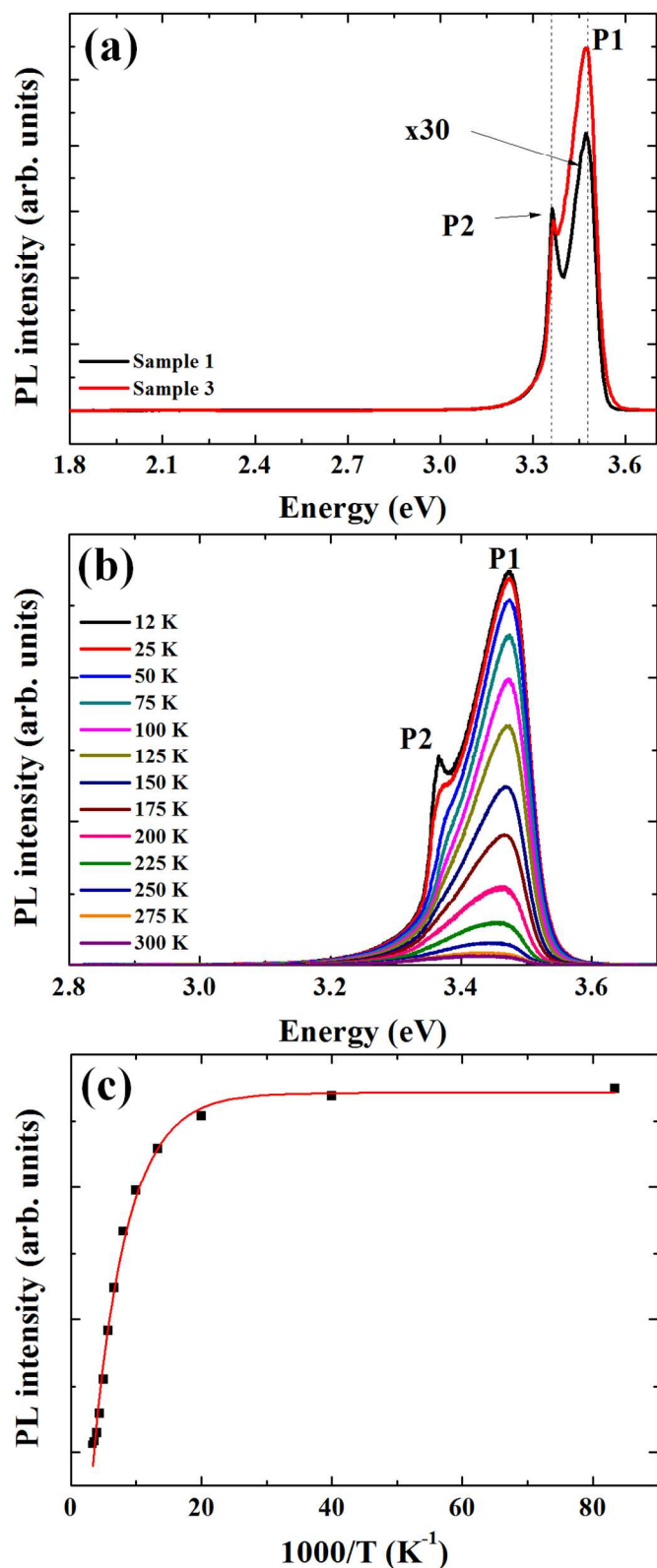


Fig. 7 (a) PL spectra at 12 K of samples 1 and 3, (b) temperature-dependent PL spectra of NBE emissions of sample 3, and (c) dependence of the integrated PL intensity on temperature. The solid line is a fit to the experimental data using Eq. (8).

Fig. 6 shows the normalized PL spectra of the $\text{Mg}_x\text{Zn}_{1-x}\text{O}$ nanorods with various Mg contents from $x = 0.20$ to $x = 0.30$ using VC-FTFA at 700 °C. The inset shows the PL spectrum of ZnO films ($x = 0$) annealed in open air at 700 °C. The NBE emission peak transfers from 3.288 to 3.519 eV as the Mg^{2+} content increases in the nanorods. The blue-shift is caused by the increase of bandgap energy due to the replacement of Zn^{2+} by Mg^{2+} . Our results are similar to the previous report.²⁴

Fig. 7a shows the PL spectra of the samples 1 and 3 measured at 12 K. Two distinct NBE emission peaks appeared at 3.474 (P1) and 3.364 eV (P2), which were attributed to the emission of neutral-donor-bound excitons (D^0X) of $\text{Mg}_{0.25}\text{Zn}_{0.75}\text{O}$ and ZnO, respectively. The intensity ratio of P1 to P2 ($I_{\text{P1}}/I_{\text{P2}}$) is larger for sample 3 than for sample 1. In order to study the origin of the UV emission in the sample 3, PL spectra were measured at various temperatures from 12 to 300 K, as shown in Fig. 7b. The intensity of the PL peak at 3.474 eV decreased with increasing temperature from 10 to 300 K because of the thermally induced dissociation of electron-hole pairs. The free excitons (FX) and D^0X are usually mixed because of the abundance of D^0X in $\text{Mg}_{0.25}\text{Zn}_{0.75}\text{O}$. However, the FX emission becomes dominant above 70 K, indicating that it is more probable for the bound excitons to be ionized and eventually become FX as the temperature increases. Fig. 7c shows the peak intensity of P1 as a function of the inverse temperatures, which decayed according to the following expression:²⁵

$$I = I_0/[1 + C\exp(-\Delta E_A/k_B T)], \quad (8)$$

where I and I_0 are the integrated intensities of the emission band, C is constant, k_B is Boltzmann's constant, and ΔE_A is the activation energy for thermal quenching. The best fit yields an activation energy of about 57 meV above 75 K, which is almost identical to the exciton binding energy of ZnO (60 meV). Therefore, the peak in the P1 in temperature range from 75 to 300 K can be attributed to the FX emission of the $\text{Mg}_{0.25}\text{Zn}_{0.75}\text{O}$ alloy by neglecting the influence of Mg incorporation on the exciton binding energy of ZnO.

Conclusions

In summary, $\text{Mg}_{0.25}\text{Zn}_{0.75}\text{O}$ nanorods prepared using the VC-FTFA method exhibit enhanced optical properties with respect to $\text{Mg}_{0.25}\text{Zn}_{0.75}\text{O}$ films annealed in open air. Sample 1 consisted of numerous round-shaped $\text{Mg}_{0.25}\text{Zn}_{0.75}\text{O}$ nanoparticles of approximately 50 nm in diameter. Large $\text{Mg}_{0.25}\text{Zn}_{0.75}\text{O}$ particles (~200 nm) were formed on the $\text{Mg}_{0.25}\text{Zn}_{0.75}\text{O}$ nanoparticles in sample 2, and $\text{Mg}_{0.25}\text{Zn}_{0.75}\text{O}$ nanorods were grown using the VC-FTFA method in sample 3. These large particles and nanorods were assembled from the round-shaped $\text{Mg}_{0.25}\text{Zn}_{0.75}\text{O}$ nanoparticles because of the role of the nucleation agents in the seed layer. The regrowth of the $\text{Mg}_{0.25}\text{Zn}_{0.75}\text{O}$ films is caused by a chloride-containing dopant such as magnesium chloride hexahydrate, which generates ZnCl_2 and MgCl_2 vapors. The NBE emission intensity was enhanced by VC-FTFA, by a factor of 37 compared to that of the films annealed in open air. The VC-FTFA method is expected to represent a possible route for the low-cost fabrication of optoelectronic devices.

The conclusions section should come at the end of article, before the acknowledgements.

Acknowledgements

This research was supported by Basic Science Research Program through the National Research Foundation of Korea (NRF) funded by the Ministry of Education, Science and Technology (No. 2012R1A1B3001837). This research was also supported by Global Ph.D. Fellowship Program through the National Research Foundation of Korea (NRF) funded by the Ministry of Education (No. 2014H1A2A1018051).

Notes and references

^a Department of Nano Science & Engineering, Inje University, 197, Inje-ro, Gimhae-si, Gyeongsangnam-do 621-749, Korea

^b Holcombe Department of Electrical and Computer Engineering, Center for Optical Materials Science and Engineering Technologies, Clemson University, Clemson, SC 29634, USA

- 1 H. Yin, Q. Wang, S. Geburt, S. Milz, B. Ruttens, G. Degutis, J. D'Haen, L. Shan, S. Punniyakoti, M. D'Olieslaeger, P. Wagner, C. Ronning and H.-G. Boyen, *Nanoscale*, 2013, **5**, 7046.
- 2 X. Liu, Q. Zhang, G. Xing, Q. Xiong and T. C. Sum, *J. Phys. Chem. C*, 2013, **117**, 10716.
- 3 S. Li, C. Zhang, F. Li, W. Ji, P. Li, M. Ren, P. Wang and M. Yuan, *RSC Adv.*, 2014, **4**, 24399.
- 4 R. Yu, C. Pan, J. Chen, G. Zhu and Z. L. Wang, *Adv. Funct. Mater.*, 2013, **23**, 5868.
- 5 S. N. Mohammad, *Nanotechnology*, 2013, **24**, 455201.
- 6 H. Nguyen, C. T. Quy, N. D. Hoa, N. T. Lam, N. V. Duy, V. V. Quang and N. V. Hieu, *Sens. Actuators B: Chem.*, 2014, **193**, 888.
- 7 M. N. Makhonin, A. P. Foster, A. B. Krysa, P. W. Fry, D. G. Davies, T. Grange, T. Walther, M. S. Skolnick and L. R. Wilson, *Nano Lett.*, 2013, **13**, 861.
- 8 Q. Yang, Y. Liu, C. Pan, J. Chen, X. Wen and Z. L. Wang, *Nano Lett.*, 2013, **13**, 607.
- 9 J.-W. Kang, Y.-S. Choi, B.-H. Kim, C. G. Kang, B. H. Lee, C. W. Tu and S.-J. Park, *Appl. Phys. Lett.*, 2014, **104**, 051120.
- 10 H. Park, G. Nam, H. Yoon, J. S. Kim, J.-S. Kim and J.-Y. Leem, *Electron. Mater. Lett.*, 2013, **9**, 497.
- 11 J. Singh, P. Kumar, N. H. Hui, J. Jung, R. S. Tiwari and O. N. Srivasatva, *RSC Adv.*, 2013, **3**, 5465.
- 12 M. Kim, Y. J. Hong, J. Yoo, G.-C. Yi, G.-S. Park, K. Kong and H. Chang, *Phys. Stat. Sol (RRL)*, 2008, **2**, 197.
- 13 J. Peng, J. Guo, S. Ding, Q. Xu, H. Li, X. Tan and X. Zhao, *Rare Metals*, 2011, **30**, 292.
- 14 Y. W. Heo, M. Kaufman, K. Pruessner, D. P. Norton, F. Ren, M. F. Chisholm and P. H. Fleming, *Solid State Electron.*, 2003, **47**, 2269.
- 15 S. Ju, J. Li, N. Pimparkar, M. A. Alam, R. P. H. Chang and D. B. Janes, *IEEE T. Nanotechnol.*, 2007, **6**, 390.
- 16 S. S. Cetin, I. Uslu, A. Aytimur and S. Ozcelik, *Ceram. Int.*, 2012, **38**, 4201.
- 17 P. Chandrasekaran, P. Anandan and N. Srinivasan, *Spectrochim. Acta A*, 2013, **116**, 311.
- 18 L. Xu, J. Su, Y. Chen, G. Zheng, S. Pei, T. Sun, J. Wang and M. Lai, *J. Alloys Compd.*, 2013, **548**, 7.
- 19 N. Guo, X. Q. Wei, R. R. Zhao and X. J. Xu, *Appl. Surf. Sci.*, 2014, **317**, 400.
- 20 H. Kanber, R. J. Cipolli, W. B. Henderson and J. M. Whelan, *J. Appl. Phys.*, 1985, **57**, 4732.
- 21 Y. G. Wang, S. P. Lau, X. H. Zhang, H. H. Hng, H. W. Lee, S. F. Yu and B. K. Tay, *J. Cryst. Growth*, 2003, **259**, 335.
- 22 C.-C. Lin and Y.-Y. Li, *Mater. Chem. Phys.*, 2009, **113**, 334.
- 23 K. H. Tam, C. K. Cheung, Y. H. Leung, A. B. Djuricic, C. C. Ling, C. D. Beling, S. Fung, W. M. Kwok, W. K. Chan, D. L. Phillips, L. Ding and W. K. Ge, *J. Phys. Chem. B*, 2006, **110**, 20865.
- 24 J. L. Morrison, J. Huso, H. Hoeck, E. Casey, J. Mitchell, L. Bergman and M. G. Norton, *Appl. Phys. Lett.*, 2008, **104**, 123519.
- 25 P. S. Venkatesh, S. Balakumar and K. Jeganathan, *RSC Adv.*, 2014, **4**, 5030.

